Assessing watershed hydrological response to climate change based on signature indices

Atiyeh Fatehifar, Mohammad Reza Goodarzi, Seyedeh Sima Montazeri Hedesh and Parnian Siahvashi Dastjerdi

ABSTRACT

Due to the fact that one of the important ways of describing the performance of basins is to use the hydrological signatures, the present study investigates the effects of climate change using the hydrological signatures in Azarshahr Chay basin, Iran. To this end, the Canadian Earth system model (CanESM2) is first used to predict future climate change (2030–2059) under two Representative Concentration Pathways (RCP2.6 and RCP8.5). Six signature indices were extracted from flow duration curve (FDC) as follows: runoff ratio (RR), high-segment volume (FHV), low-segment volume (FLV), mid-segment slope (FMS), mid-range flow (FMM), and maximum peak discharge (DiffMaxPeak). These signature indices act as sorts of fingerprints representing differences in the hydrological behavior of the basin. The results indicate that the most significant changes in the future hydrological response are related to the FHV and FLV and FMS indices. The BiasFHV index indicates an increase in high discharge rates under the RCP8.5 scenario, compared to the baseline period, and also the RCP2.6 scenario. The mean annual discharge rate, however, is lower than the discharge rate under this scenario. Generally, for the RCP8.5 scenario, the changes in the signature indices in both high discharges and low discharges are significant.

Key words | flow duration curves (FDC), RCP scenarios, signature biases, streamflow changes, SWAT

Atiyeh Fatehifar
Mohammad Reza Goodarzi (corresponding author)
Seyedeh Sima Montazeri Hedesh
Parnian Siahvashi Dastjerdi
Department of Civil Engineering,
Yazd University,
Yazd,
Iran
E-mail: *goodarzimr@yazd.ac.ir*

HIGHLIGHTS

- Prediction of future runoff under two RCPs using SDSM and SWAT models.
- Six signature indices were used to investigate the hydrological behavior of the basin.
- Annual precipitation, temperature, streamflow and six signature indices of the RCPs were compared.
- The most significant changes in the future of hydrological response are related to high flows.

doi: 10.2166/wcc.2021.293

GRAPHICAL ABSTRACT

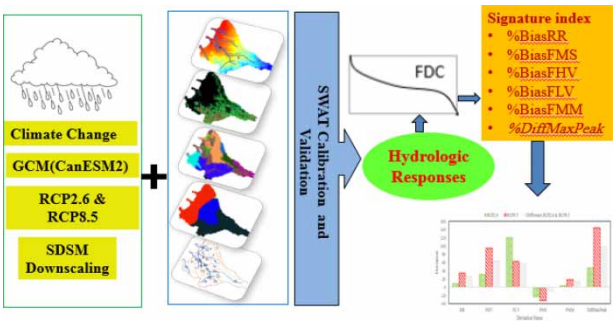

INTRODUCTION

The world is presently facing rapid climate changes. One of the main concerns of hydrologists is comprehension and prediction of related hydrologic changes. Therefore, it is necessary to precisely map the changes in hydrologic response of catchments (Casper *et al.* 2011). Hydrological signatures are designed to extract information about changes in the hydrologic response of catchments. Hydrological signatures are index values derived from observed or simulated series of hydrological data (McMillan *et al.* 2017). Hydrologic signatures are quantitative metrics that extract and summarize the information contained in streamflow. Generally, signature indices can be categorized into three main areas: (1) ecohydrology, environmental flows and hydrologic alteration, (2) watershed processes, and (3) modeling (McMillan 2020).

Signature indices have long been used in hydrological analyses (Westerberg *et al.* 2016), but the concept of a hydrological signature was first explicitly described by Gupta *et al.* (2008) in the context of deriving minimal representations of the relevant information contained in a hydrological dataset (Gupta *et al.* 2008; McMillan *et al.* 2017). They reported that hydrological signatures can be defined as the results of data analysis which provide information about hydrological performance of a watershed according to system behavior interpretation. For instance, signatures are used to detect hydrological change (Westerberg & McMillan 2015). Signatures can also be used to draw hydrological analogies between catchments (McDonnell & Woods 2004; Wagener *et al.* 2007; Sawicz *et al.* 2011) and contribute to prediction of signature values in ungauged catchments (Blöschl *et al.* 2013). Some authors have considered the effect of data uncertainty on hydrological signatures (Kauffeldt *et al.* 2013). Juston *et al.* (2014) investigated the impact of rating curve uncertainty on flow duration curves (FDCs) and change detection for a Kenyan basin. They showed that uncertainty in extrapolated high flows creates significant uncertainty in the FDC and the total annual flow (Juston *et al.* 2014; Westerberg & McMillan 2015). In their study, Casper *et al.* (2011) proposed nine hydrological signature indices which were applied on the outputs of a hydrologic basin model introduced for three different catchments (western Germany) to find distinctions among various meteorological input data. According to the data-driven graphs, signatures with high bias values are indicative of the fact that the Consortium for Small-scale Model (COSMO or CCLM) has not been calibrated. They concluded that signature indices can act as indirect 'efficiency measures' or 'similarity measures' on output from regional climate models and the control period of the simulation. Westerberg *et al.* (2016) investigated signature uncertainty in 43 UK catchments. In their study, they used two signature classes: signatures measuring flow distribution and signatures measuring flow dynamics. They used the regionalization method to evaluate the role and relative magnitude of the uncertainties. In the uncertainty distribution, the predicted signatures were considered as ungauged data. They found that uncertainty in the regionalization results was lower for signatures measuring flow distribution (e.g.,

Qmean) than flow dynamic. Nevertheless, the link between signature values and hydrological behavior and processes is not always straightforward, causing hydrologists' signature choices to be associated with uncertainty and variability. Each chosen signature should be able to present the objectives of the study. Five criteria are used to measure this ability. In fact, an acceptable signature should have most or all of the criteria.

Previous studies have shown that signature indices have been employed for various aims such as monitoring change in hydrologic systems, analyzing runoff, defining similarity between basins, and model calibration and evaluation. Actually, hydrological signatures are indicators that describe catchment behavior relating to hydrological processes and catchment performance. The signature indices used in this article are chosen based on the five criteria (identifiability, robustness, consistency, representativeness, discriminatory power). The chosen signature indices allow assessment of changes in water balance, vertical water distribution, reactivity, and extreme events. Although the study by Goodarzi *et al.* (2020) has investigated the effect of climate change on flood in Azarshahr basin, in this study, the hydrological response is investigated by the signature indices in the basin. The objectives of the present study are as follows: (1) investigation of the climate change effects on streamflow in Azarshahr Chay catchment in the future (2030–2059) under Representative Concentration Pathways (RCP2.6 and RCP8.5) and (2) once suitable signatures are selected based on the aforementioned five criteria, changes in the hydrological behavior of the catchment are investigated under two climatic scenarios in the future (2030–2059). In general, the main difference between the present study and other related studies lies in the use of these signatures. Since most works in the literature on signature indices are used to model calibration and validation (Yilmaz *et al.* 2008; Juston *et al.* 2014; Westerberg *et al.* 2016) or to affect different regional climate models' resolution (RCM) (Casper *et al.* 2011; Mendoza *et al.* 2016), the present study uses the general circulation model (GCM) and new RCP scenarios (according to Fifth Assessment Report Intergovernmental Panel on Climate Change (IPCC)) for climate simulation. In addition, the Soil and Water Assessment Tool (SWAT) model, which is known as a continuous and semi-distributed model, and the SWAT-CUP are used to model calibration and validation, respectively. The hydrological signature index has been used to evaluate the flow biases in the baseline period relative to the future period.

MATERIALS AND METHODS

Study area

Azarshahr Chay basin is one of the fourth-order sub-basins in northwestern Iran. This basin covers an area of 702 km^2 and is situated southwest of Tabriz city. Figure 1 shows the location of the basin. The basin is characterized by an average annual precipitation of 266.21 mm and an average annual temperature of about 13.22 °C. Tmin, Tmax, and precipitation obtained from two meteorological stations (1976–2005) were used in the present study. Solar radiation, wind speed, and relative humidity which were simulated by the SWAT model were among other meteorological data used in the study. Azarshahr hydrometric station and the observed streamflow changes in the basin were used for calibration and verification purposes (Figure 1 and Table 1).

Climate change and downscaling

GCMs are the most important instruments used to predict global and continental climate change variables. The Canadian Earth System Model (CanESM2), designed by the Canadian Centre for Climate Modelling and Analysis, was used in the present study. CanESM2 has a resolution of 2.81° latitude × 2.81° longitude and covers four RCP scenarios, namely, RCP2.6, 4.5, 6, and 8.5 from 2005 to 2100 as well as National Centers for Environmental Prediction (NCEP) data from 1961 to 2005 (Pervez & Henebry 2014). These scenarios are designed based on results of socio-economic and technological studies as well as the concentration of some gases in the decades to come. In the RCP2.6 and RCP8.5 scenarios, the effect of lowest CO_2 emissions (490 ppm) and highest GHG emissions (1,370 ppm) on radiation retention is projected to be 2.6 W/m^2 and 8.5 W/m^2 by 2100, respectively (IPCC 2014; Khan & Koch 2018).

The output of GCMs cannot, due to their large scale or high spatial resolution, be used on a regional or local scale. Therefore, it is necessary to establish a quantitative

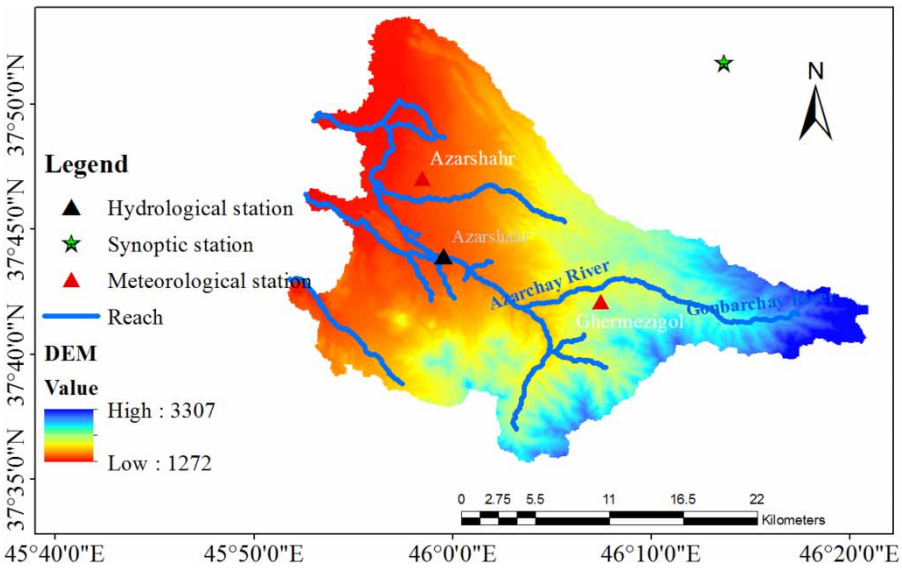

Figure 1 | Location of the basin.

Table 1 | Specifications of stations in the study area

Station name	Longitude	latitude	Elevation	Observed variable	Base period
Azarshahr	45°57′0″	37°47′0″	1,340	Daily (Tmin, Tmax, P)	1976–2005
Ghermezigol	46°6′0″	37°44′0″	1,673	Daily (P)	1976–2005
Azarshahr	45°59′0″	37°45′60″	1,425	Q	1976–2005

relationship between large-scale variables of general circulation model and the small-scale observational variables (local or regional) (Wilby *et al.* 2006). This relationship is presented in the following equation (Dibike & Coulibaly 2005):

$$Y = f(X) \quad (1)$$

where Y is the predictor variable, X is the predictand variable, and f is the transfer function, which is experimentally derived from observational data. In the present study, the statistical downscaling model (SDSM) was used to downscale the Tmax and Tmin and precipitation data from 1976 to 2005. SDSM is an instrument presented by Wilby *et al.* (2002) to assess the regional/local climate change impacts. This method has four elemental steps that include (1) selection of predictor variables, (2) calibration of the model (using observed predictors), (3) validation of the model, and (4) generation of future scenarios (using climate model predictors). In this study, data were downloaded from http://climate-scenarios.canada.ca/?page=pred-canesm2 with the location of the cell 17 x and 46 y. The large-scale variables, derived from NCEP, are defined as independent variables and dependent variables and include precipitation and maximum and minimum temperatures, observed daily and defined in the SDSM model. NCEP variables contain 26 atmospheric parameters (Table 2), from which independent variables are selected. One of the most important steps in statistical downscaling is selecting the dominant variables – containing the highest correlation coefficient and the lowest error variance – as model characteristics, and the results are influenced directly by these variables. The dominant variables should have a high statistical correlation and physical relation to the dependent variables (Wilby *et al.* 2002).

Table 2 | The 26 used NCEP predictor variables

No.	Predictors	Abbreviation	No.	Predictors	Abbreviation
1	Mean sea level pressure	mslp	14	500 hPa divergence	p5zh
2	Surface airflow strength	P-f	15	850 hPa airflow strength	p8_f
3	Surface zonal velocity	P-u	16	850 hPa zonal velocity	p8_u
4	Surface meridional velocity	p-v	17	850 hPa meridional velocity	p8_v
5	Surface vorticity	p-z	18	850 hPa vorticity	p8_z
6	Surface wind direction	p_th	19	850 hPa geopotential height	p850
7	Surface divergence	p_zh	20	850 hPa wind direction	p8th
8	500 hPa airflow strength	p5_f	21	850 hPa divergence	p8zh
9	500 hPa zonal velocity	p5_u	22	500 hPa relative humidity	r500
10	500 hPa meridional velocity	p5_v	23	850 hPa relative humidity	r850
11	500 hPa vorticity	p5_z	24	Surface relative humidity	Rhum
12	500 hPa geopotential height	p500	25	Surface specific humidity	Shum
13	500 hPa wind direction	p5th	26	Near-surface temperature	Temp

Runoff simulation using the SWAT model

SWAT is a physically based, continuous, semi-distributed hydrological model. Numerous studies carried out in the international arena have proven the high accuracy of the model (Zhang *et al.* 2016). In the SWAT model, the watershed is divided into a number of sub-basins based on the digital elevation model (DEM). In the next step, the watershed is further subdivided into smaller units known as hydrological response units (HRUs) based on land use, soil class, and slope class. These units should be hydrologically uniform in terms of soil characteristics, topography, land cover and land use. The water balance equation in this model is as follows:

$$SWt = SW_{\mathrm{o}} + \sum_{i-1}^{t} (Rday - Qsurf - Ea - Wseep - Qgw)i \quad (2)$$

where SWt is the final soil water content (mm), SW_{o} is the initial soil water content (mm) (up to a depth of 60 cm), t represents time in days, $Rday$ denotes precipitation on day i (mm), $Qsurf$ represents surface runoff on day i (mm), Ea is the level of evapotranspiration on day i (mm), $Wseep$ is the amount of water entering the unsaturated zone from the soil profile on day i (mm), and Qgw is the amount of return flow (mm) (Zhang *et al.* 2016).

The SUFI2 algorithm was used in the SWAT-CUP software to improve the calibration quality and analysis of uncertainty in the model results. The SUFI2 algorithm combines calibration and uncertainty and tries to determine the uncertainty parameters in such a way that the observational data mostly fall within the pre-determined uncertainty zone. In the meantime, it tries to create the narrowest possible uncertainty spectrum. Therefore, optimal conditions are realized when: (1) most of the observational data are bracketed by 95% prediction uncertainty (95-PPU) band (P-factor → 1) and (2) the average distance between the upper and lower boundaries, in 95% prediction uncertainty (95-PPU) divided by the standard deviation of the measured data (R-factor → 0) is as small as possible (Abbaspour *et al.* 2009). Aside from the uncertainty parameters, two other statistical indices, namely, coefficient of determination (R^2) and Nash–Sutcliffe efficiency (NSE) are used for calibration and validation purposes.

In the present study, meteorological information including daily precipitation, as well as daily Tmax and Tmin (1981–1989) were introduced into the model and other meteorological information was simulated by the model. The curve number method, variable storage method, and Hargreaves–Samani method were used to estimate surface runoff, carry out flow routing, and determine evapotranspiration, respectively. Azarshahr hydrometric station was

used as the base station to observe the runoff variations in the basin.

Signature indices

Signature indices provide information that can be used to diagnose and isolate the causes of model inadequacy thereby providing guidance towards model improvement (Yilmaz *et al.* 2008). Unlike standard statistical criteria, signature indices have their roots in the framework of hydrological theory that underlies our conceptual representation of the watershed. The reason for multiplicity of indices is that each index is designed to address different (complementary) aspects of the model/system behavior (Gupta *et al.* 2008; Herbst *et al.* 2009). Following the mathematical concepts and formulas presented by Yilmaz *et al.* (2008), authors actually shifted their focus to various signature indices that provide information on the intrinsic properties, including total water equilibrium, redistribution of soil moisture, and long-run behavior of base flow (Herbst *et al.* 2009). Selection of appropriate hydrological signatures based on modeling objectives is actually tantamount to estimation of water equilibrium and availability of the observed data. These signatures have been selected based on five features of a suitable signature. (1) Identifiability: signature value uncertainties should be small relative to the range of values between different catchments (Westerberg *et al.* 2016). In fact, an uncertainty estimate should be cited alongside all signature values (Westerberg & McMillan 2015). (2) Robustness: ensures that the signature describes the catchment itself rather than the measurement of the catchment. (3) Consistency: signature values should be comparable across catchments, and insensitive to irrelevant factors. This characteristic can frequently be incorporated into the signature design, such as normalization by catchment area, to maximize the usefulness of the signature in comparing catchments according to underlying hydrological function rather than superficial catchment characteristics (Mcmillan *et al.* 2017). (4) Representativeness: hydrological properties are frequently heterogeneous at small scales, whereas modeling or management applications require estimates of emergent catchment-scale behavior. Therefore, signatures should describe average (sub-) catchment behavior. This implies that signature values should vary almost linearly with the underlying descriptor. (5) Discriminatory power: according to this criterion, knowledge of signature values is meant to add to our knowledge of hydrological function. Hence, it can be argued that differences in signature values should increase as differences in hydrological function increase. This index is also used in a modeling-specific sense, such that a constraint on the signature must reduce the prediction range of feasible models (Schaefli *et al.* 2011; Mcmillan *et al.* 2017). Furthermore, a signature should relate only to a subset of model parameters (Yilmaz *et al.* 2008).

Some signatures represent the long-term input–output behavior of the basin (BiasRR%) or runoff of different magnitudes (%*BiasFHV*, % *BiasFLV*, % *BiasFMM* %.) (Gunkel *et al.* 2015). These indices that are extracted from FDC serve as fingerprints that indicate differences in the hydrological behavior of the basins. FDC indicates the cumulative probability distribution function of the flow. In this curve, the magnitude of flow stands in contrast to maximum probability of it. In fact, an FDC is one of the most informative methods of displaying the complete range of river discharges ranging from low flows to flood events. It is a relationship between any given discharge value and the percentage of time that this discharge is equaled or exceeded, or in other words – the relationship between magnitude and frequency of streamflow discharges (Smakhtin 2001). In the present paper, daily data are used to calculate FDCs. The calculated signatures used to study the basin are introduced below.

The first signature index focuses on the long-term input–output behavior of the system (volume balance), and therefore measures the percent bias in overall runoff (% BiasRR). This index is strongly controlled by the evapotranspiration process and any factor that influences the quantity of water available for evapotranspiration. The index should, therefore, be sensitive to the model components and parameters that control these processes (Herbst *et al.* 2009). BiasRR presented in Equation (3) indicates differences' bias in water balance (Yilmaz *et al.* 2008):

$$\%BiasRR = \frac{\sum_{h=1}^{H} (Qs_h - Qo_h)}{\sum_{h=1}^{H} (Qo_h)} \times 100 \quad (3)$$

In this equation, h denotes the probability percentage row number and H represents the last row number in the 0–100% probability range, while Qsh and Qoh denote simulated and observed flow, respectively.

BiasFMS represents the percent bias in FDC mid-segment. It is actually used to measure vertical redistribution. t and h presented in Equation (4) denote the 20 and 70% probabilities, respectively (Yilmaz *et al.* 2008):

$$\%BiasFMS = \frac{(\log Qs_t - \log Qs_h) - (\log Qo_t - \log Qo_h)}{(\log Qo_t - \log Qo_h)} \times 100 \quad (4)$$

BiasFHV is the percent bias in FDC high-segment volume where $h = 1,2, \ldots, H$ is the flow index for flows with exceedance probabilities between 0 and 2% (Yilmaz *et al.* 2008). In fact, FDC is used to diagnose a series of useful features. This property is measured as the percentage of error in the high-segment volume of FDC (Equation (5)):

$$\%BiasFHV = \frac{\sum_{h=1}^{H} (Qs_h - Qo_h)}{\sum_{h=1}^{H} Qo_h} \times 100 \quad (5)$$

In the BiasFLV, $h = 1, 2, \ldots, H$ denote the flow indices in FDC low-segment volume (probabilities between 70 and 100%), that is (row number), from 70% probability to H that denotes minimum flow index which is equal to the 100% probability row number (Yilmaz *et al.* 2008). In this signature, the indices show all discharge values with a probability exceeding 0.02. Similarly, the volume of water corresponding to the long-term base flow is measured as the percent bias in the FDC low-segment that is denoted by %BiasFLV (Equation (6)):

$$\%BiasFLV = \frac{\sum_{h}^{H} (\log Qs_h - \log Qs_H) - \sum_{h}^{H} (\log Qo_h - \log Qo_H)}{\sum_{h}^{H} (\log Qo_h - \log Qo_H)} \times 100 \quad (6)$$

BiasFMM uses the log transform of the flow to increase sensitivity to very low flows. In fact, this index should be sensitive to components/parameters that influence base flow recession rates, as well as those that control the demand for evapotranspiration loss from the stream and/or the lower zone storage. The signature is measured based on FDC, the percentage of bias in the mid-segment of the curve with the flow converted to log. This FDC-based signature is measured based on the percentage of bias in median of the log transformed discharges %BiasFMM: (Yilmaz *et al.* 2008):

$$\%BiasFMM = \frac{medianQs - medianQo}{medianQo} \times 100 \quad (7)$$

DiffMaxPeak denotes the percentage of error at maximum peak discharges with the index number of the highest element of the FDC being (Herbst *et al.* 2009):

$$\%DiffMaxPeak = \frac{Qmax(s) - Qmax(o)}{Qmax(o)} \times 100 \quad (8)$$

where o and s represent the observed and simulated discharges, respectively.

Output indices of the FDC are recognized as watershed characteristics that operate on short- to medium-timescale.

FDC shows the tendency of the catchment to generate different resources as well as the vertical redistribution of soil moisture. Therefore, different segments of the curve are associated with fast, medium, and slow reactions, and the FDC model requires the removal of scheduling information (Herbst *et al.* 2009). The list of signatures used in the present study is presented in Table 3.

Table 3 | Description of signatures used in this study

Signature name	Description
BiasRR	Runoff ratio indicates the differences in water balance
BiasFHV	Percent bias in high-segment volumes which compares the peak discharges
BiasFLV	Percent bias in low-segment volumes (deference in long-term baseflow)
BiasFMS	Percent bias in mid-range flow levels
BiasFMM	The diagnostic signature measures for vertical redistribution are the percent bias in FDC midsegment slope (Yilmaz *et al.* 2008)
DiffMaxPeak	The percentage of error in maximum peak discharge (Herbst *et al.* 2009)

Model performance

Root mean square error (RMSE), determination coefficient (R^2), and Nash–Sutcliffe efficiency (NSE) are used to check the reliability of the simulated data in SDSM and SWAT models.

$$RMSE = \sqrt{\frac{\sum_{i=1}^{n}(O_i - S_i)^2}{n}} \quad (9)$$

$$R^2 = \frac{\left[\sum_{i=1}^{n}(O_i - \bar{O}).(S_i - \bar{O})\right]^2}{\sum_{i=1}^{n}(O_i - \bar{O})^2 . \sum_{i=1}^{n}(S_i - \bar{S})^2} \quad (10)$$

$$NSE = 1 - \frac{\sum_{i=1}^{n}(S_i - O_i)^2}{\sum_{i=1}^{n}(O_i - \bar{O})^2} \quad (11)$$

where $\bar{O}$ denotes the mean observed data, $\bar{S}$ is the mean simulated data, O_i represents the observed data in the entire period and S_i denotes the simulated data in the entire period, n is the total number of data.

RESULTS AND DISCUSSION

The SDSM model and climate change results

The SDSM model was calibrated and validated prior to simulation of future climate change. In this process, the observational data were evaluated and subjected to quality control processes, and then the NCEP predictors with the highest correlation with each of the observational data were selected. The Tmin and Tmax of Azarshahr station for the calibration period 1990–2000 and validation period 2001–2005 as well as the precipitation data of Azarshahr and Ghermezigol stations for the periods 1976–1995 and 1996–2005 were simulated for calibration and validation purposes, respectively. The NCEP variables with highest correlation coefficient in the SDSM model are shown in Table 4 The model performance results obtained using R^2, NSE, and RMSE coefficients are presented in Table 5 for both calibration and validation periods. As Table 5 shows, R^2 and NSE coefficients obtained in calibration and validation periods are highly consistent and close to 1, which shows optimal performance and high simulation accuracy of the model. In the calibration period, R^2, NSE, and RMSE coefficients were in the 0.86–0.99, 0.82–0.99, and 0.68–1.83 range, respectively. In the validation period, however, these coefficients were in the 0.78–0.98, 0.72–0.98, and 0.56–2.04 range, respectively. Once a reasonable relation between the model and obtained data was achieved, the future simulation was performed.

In the next step, the SDSM downscaling accuracy was first evaluated and then the future climate was simulated using the CanESM2 model under RCP2.6 and RCP8.5 scenarios. The range of future temperature and precipitation variations are presented in Table 6. Figure 2 shows the monthly temperature changes in Azarshahr station (1990–2005) and precipitation changes in Azarshahr and Ghermezigol stations (1976–2005) in the baseline period as

Table 4 | Selection of atmospheric predictors for downscaling

Variables	Tmax	Tmin	p
Ncepp500gl	√		
Nceptempgl	√	√	√
Ncepp850gl		√	
Ncepp1ugl			√
Ncepp5thgl			√
Ncepp5fgl			√
Ncepp5zgl			√
Ncepp850gl			√
Ncepp8vgl			√
Ncepp5vgl			√

Table 5 | The performance of the SDSM model for calibration and validation periods

Performance statistics		Tmax	Tmin	Precipitation Azarshahr	Precipitation Ghermezigol
Calibration	R^2	0.99	0.99	0.94	0.86
	NSE	0.99	0.99	0.93	0.82
	RMSE	1.83	1.48	0.68	0.81
Validation	R^2	0.98	0.98	0.78	0.78
	NSE	0.98	0.98	0.72	0.72
	RMSE	2.40	0.69	0.56	0.69

Table 6 | Mean annual Tmax, Tmin, and precipitation variations under RCP2.6 and RCP8.5 scenarios in future periods (relative to the baseline period)

	Temperature (°C) 1990–2005		Precipitation (%) (1976–2005)	
RCPs (2030–2059)	Tmax 18.71 °C	Tmin 7.78 °C	Azarshahr S 228.64	Ghermezigol S 287.08
RCP 2.6	+0.06	+0.13	+7.44	−1.15
RCP 8.5	+0.26	+0.23	+4.53	−7.57

compared to the future periods. Table 6 shows that the future Tmax and Tmin values have increased under both scenarios. The increase was found to be more significant under the RCP8.5 scenario and this could be attributed to pessimistic climate simulation conditions that were taken into account under this scenario. The percentage of precipitation increased and decreased at Azarshahr and Ghermezigol stations, respectively. Nevertheless, the percentage of precipitation under the RCP8.5 scenario was lower than that under the RCP2.6 scenario in both basins' hydrological response states.

According to Figure 2, the highest rise in Tmax (2.61) has occurred in July under the RCP8.5 scenario. The figure

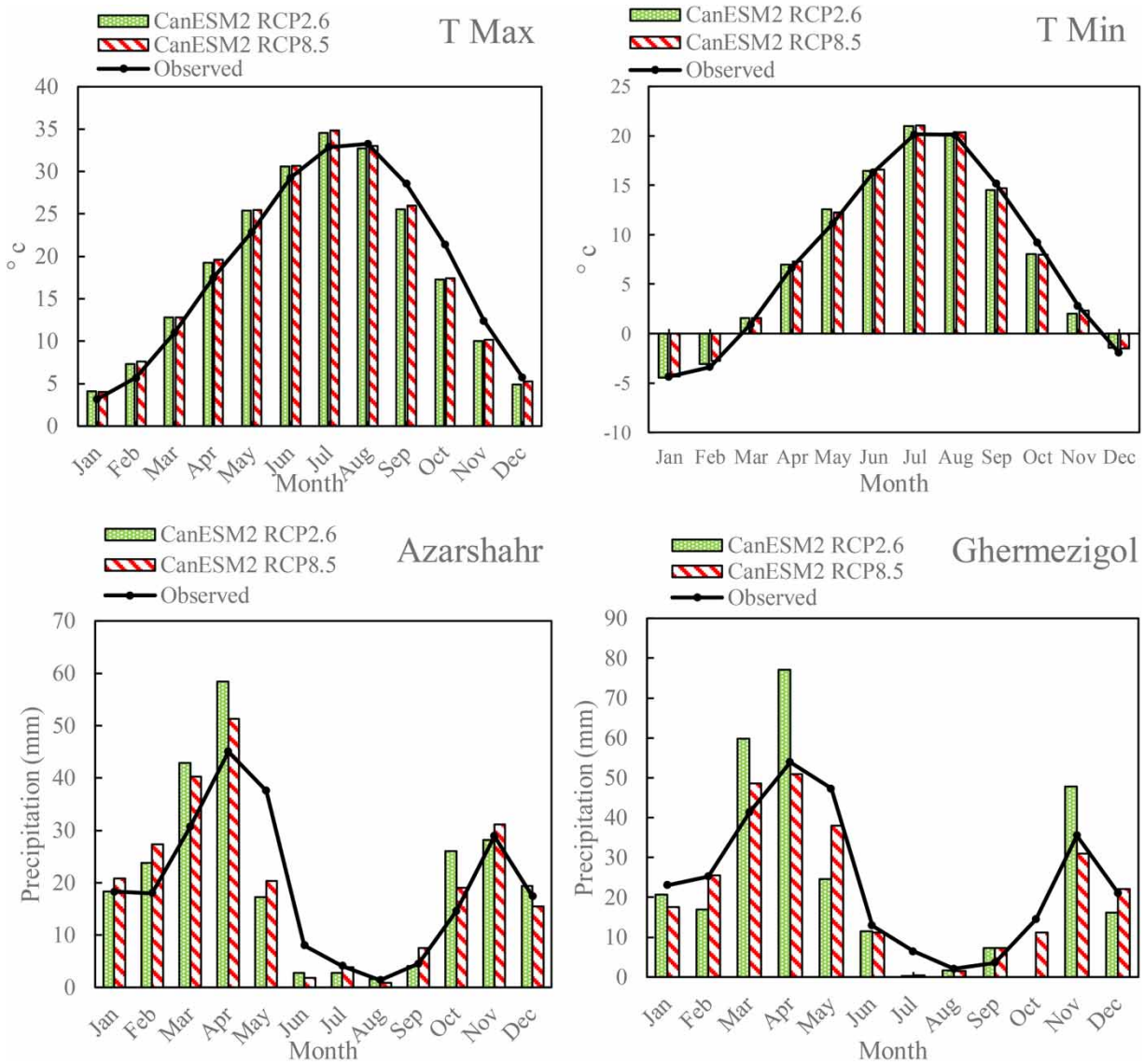

Figure 2 | Monthly Tmax, Tmin, and precipitation variations at simulated stations in baseline and future periods.

also shows that temperature reaches its maximum level during July. Maximum rise in Tmin occurs in May under both scenarios. Decline and rise in precipitation usually take place during the hot and cold months of the year, respectively. For Azarshahr and Ghermezigol stations, according to Figure 2, the rise in precipitation becomes less significant as we shift from RCP2.6 to RCP8.5.

The SWAT model and discharge variation results

The required data including DEM maps, land use, basin soil type, daily precipitation data, temperature as well as the information related to synoptic stations were introduced into the model. The HRUs were obtained after overlapping DEM, land use and soil type maps on the SWAT2012 model and defining the 10% land use threshold, 5% soil type threshold, and the 10% slope threshold. The process led to formation of 147 HRUs and division of the basin into 26 sub-basins. Once the basic model was run, the SUFI2 algorithm (with 500 model runs) in the SWAT-CUP was used to improve the flow simulation results and analyze sensitivity as well as accuracy of calibration and validation processes. Table 7 shows the optimal and effective discharge values obtained using the SWAT. The model calibration results at daily time steps during the four-year period (1984–1987) and model validation results at daily time steps during the two-year period (1988–1989) are presented in Figure 3. According to Figure 3(a), in the calibration period, R^2, NSE, P-factor, and R-factor are equal to 0.67, 0.54, 0.57, and 0.61, respectively, while in the validation period, these coefficients are equal to 0.66, 0.64, 0.63, and 0.55, respectively. Figure 3(b) shows the diagram of observed and simulated daily discharge values in the calibration and validation periods. The results are indicative of acceptable accuracy of the model in estimation of streamflow in the calibration and validation periods.

Table 7 | Calibrated SWAT parameters, their descriptions, range, and fitted values

Parameter	Description	Range	Fitted value
r_CN2.mgt	Curve number	−0.3 – 0.3	−0.24
V_GW_DELAY.gw	Groundwater delay time (days)	0–300	60.49
r_SOL_AWC.sol	Soil available water capacity (mm)	−0.2–0.4	0.22
V_ALPHA_BF.gw	Baseflow recession constant	0–1	0.30
V_ESCO.hru	Soil evaporation compensation factor	0.9–1	0.96
V_PLAPS.sub	Precipitation lapse rate	100	100
V_SMTMP.bsn	Snow melt base temperature	−3–1	−1.5
r_SOL_K.sol	Soil hydraulic conductivity, mm/hr	−0.5–0.5	−0.33
V_TLAPS.sub	Temperature lapse rate	−6–6	−1.72
V_CANMX.hru	Maximum canopy storage (mm)	5–60	20.52
V_SURLAG.bsn	Surface runoff lag time (days)	1–24	2.73
V_SMFMX.bsn	Melt factor for snow on 21 Jun	0–10	4.32

V_: 'value', this means the existing parameter value will be replaced by the given value.
r_: 'ratio', this means the existing parameter is multiplied by (1 + given value).

Future discharge changes

After making sure of the accuracy of the SWAT simulations of the basin streamflow, the downscaled time series of temperature and precipitation associated with the future period (2030–2059) were introduced into the SWAT model to obtain the future daily streamflow time series of the basin. The results are indicative of rises in the average annual streamflow. According to the results, the streamflow has increased by 3.2% and 2.1% under RCP2.6 and RCP8.5 scenarios, respectively. Figure 4 shows the monthly variations in the discharge level. Looking more closely, one can easily realize that the future river flow pattern has undergone some changes in some months of the year (compared to the 30-year observation period). In other words, the flow rate has increased from mid-October to early April period and has decreased in the period between May and September. Moreover, extreme precipitations are mostly observed in the same months of the future periods. Nevertheless, runoff has, according to the observations, increased relative to the baseline period and decreased relative to the RCP2.6 scenario.

Signature indices analysis and changes

Before analyzing the basin signatures, it is necessary to plot the FDC. Therefore, the 30-year runoff data were used to

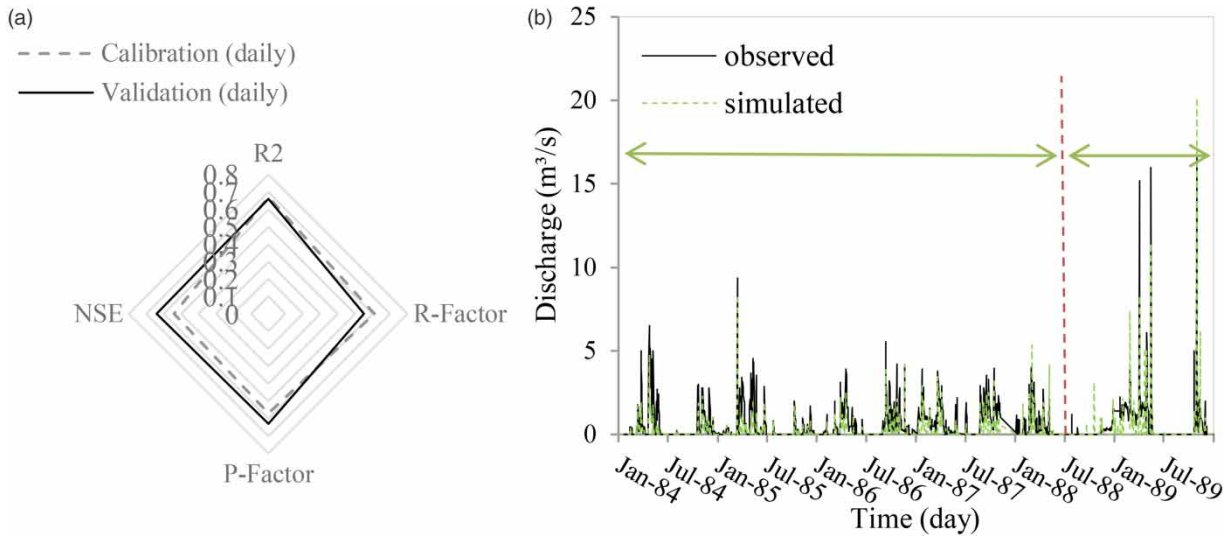

Figure 3 | (a) Evaluation indices and (b) daily-step discharge data used to test the accuracy of calibration and validation in the SWAT model.

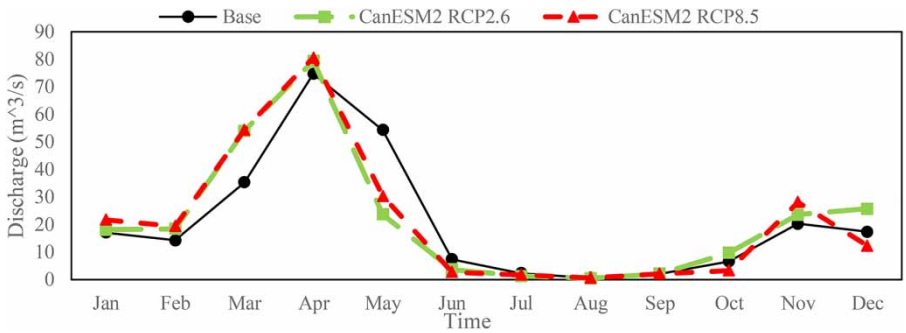

Figure 4 | Changes in average monthly runoff under climatic and baseline scenarios over a 30-year period.

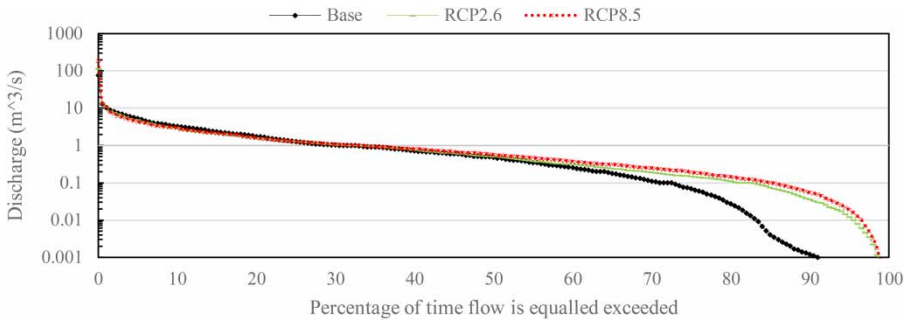

Figure 5 | Flow duration curve for base and RCPs scenarios.

plot the FDC. The FDC in the baseline period and under RCP2.6 and RCP8.5 scenarios is presented in Figure 5. This curve serves as the premise of basin signature analysis.

Every single signature was evaluated against the five intrinsic features of a good signature (identifiability, robustness, consistency, representativeness, and discriminatory power) and the scores of the signatures used for the basin in the study area were calculated according to Table 3.

Since there are two scenarios for the future, the aforementioned equations were used twice. Taking into account

the equations introduced for each of the signatures and the three available datasets, the FDC was used to obtain two discharges (the discharge under optimistic and pessimistic scenarios) for each signature. The first discharge resulted from involvement of observed and predicted data in the optimistic future scenario (RCP2.6) and the second discharge resulted from involvement of observed and predicted data in the future pessimistic scenario (RCP8.5). The optimistic and pessimistic scenarios and the difference between them for different signatures under both future scenarios (RCP2.6 and RCP8.5 (2030–2059)) are presented in Figure 6.

The chosen signature indices represent changes in water balance (BiasRR, BiasFMM), vertical water distribution (BiasFHV, BiasFLV), reactivity (BiasFDCmidslope), and extreme flows (DiffMaxPeak). Figure 6 shows that the value of BiasRR is approximately 9.26% under the RCP2.6 scenario and approximately 34.95% under the RCP8.5 scenario. Comparison of the two values and the BiasRR definition provided before shows a higher level of surface runoff under the RCP8.5 scenario. The BiasRR results demonstrate that runoff has increased as this index uses the mean of FDC. Since this is a seasonal river, an increase in the RR index does not mean a uniform increase in runoff over a 30-year period. Zero values are removed in the FDC; therefore, this index is significantly affected by high flows. Taking into account the difference of 25.68% between the two scenarios, it can be argued that the conclusion is confirmed and this variation can be attributed to differences in climatic conditions. FHV index is sensitive to severe floods and peak flow rates (exceedance probabilities lower than 0.02). The high-flow volume increases (positive index BiasFHV). The results also show that BiasFHV is approximately 31.18% under the RCP2.6 scenario and approximately 94.55% under the RCP8.5 scenario. Since this signature is provided for high-discharge flows, it can be argued that the number of high-discharge flows is higher in the pessimistic scenario (RCP8.5). This conclusion is consistent with the main hypothesis. Moreover, the difference of 63.37% between the two scenarios indicates that consideration of pessimistic conditions can lead to extreme hydrological responses and events such as floods in this signature, which is consistent with the results of increasing future flood under this scenario in the same basin (Azarshahr basin) in Goodarzi *et al.* (2020). According to this conclusion, although the average annual discharge was higher under the RCP2.6 scenario, the maximum discharge rate was still higher under the RCP8.5 scenario. These changes and findings are the result of signature investigations rather than average annual or monthly runoff studies. The BiasFLV (70–100% in FDC), was found to be 120.61% under the RCP2.6 scenario and approximately 62.88% under the RCP8.5 scenario. Since this signature is presented for low flows, it can be argued that the number of low flows is lower under the pessimistic scenario. By considering BiasFLV results, the value of the RCP2.6 scenario is higher than other scenarios. This means that, in the optimistic scenario, the low flow will be higher in the future and the runoff distribution will be uniform over the RCP8.5 scenario. Then, in the RCP2.6 scenario, fewer extreme events have occurred. Therefore, the reason why the average

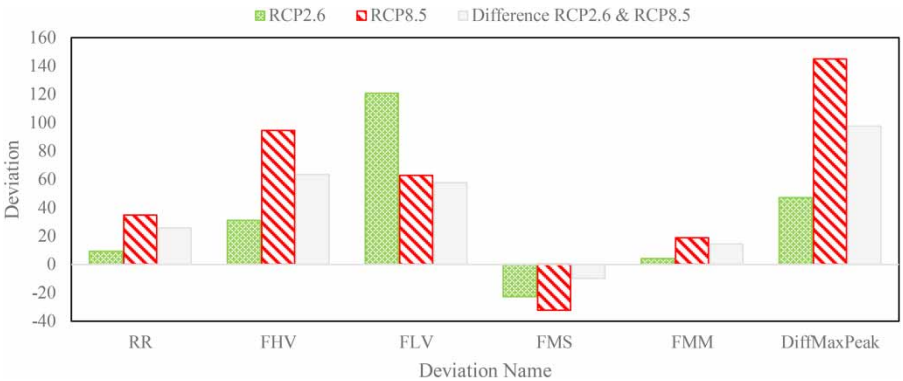

Figure 6 | Signature indices resulting from comparison of observed discharge time series (1976–2005) and RCP2.6 and RCP8.5 scenarios discharge time series (2030–2059) and difference between RCP2.6 and RCP8.5.

annual runoff (+3.2) is higher in this scenario can be justified by the low flow rate. The difference between the two scenarios is significantly high (57.73%) and this indicates that pessimistic changes in the conditions of a basin can significantly affect low discharge and high discharge. Taking this into account, it can be argued that in the RCP8.5 scenario, bias in high flows and low flows are more significant than that in the baseline and optimistic scenario, and this is indicative of an increase in extreme events such as flood and drought. The percentage of bias in the mid-segment slope of the FDC (the discharges standing between FHV and FLV discharges) which are presented as BiasFMS (exceedance probabilities between 0.2 and 0.7) in Figure 6 is approximately −22.80% under the optimistic scenario and approximately −32.43% under the RCP8.5 scenario. The FMS index, which describes the largest part of the FDC curve, shows the response of the dominant basin. The negative reactivity of the catchment can be explained by temperature rise in the future and basin behavior in the long term. The minus value of biases can be attributed to the lower value of simulated discharges compared to the observed discharges. Taking into account the small difference between these two values (9.63%), it can be argued that this signature, compared to the previous two signatures, is less significantly affected by basin condition changes under the pessimistic and optimistic scenarios and significant biases are mostly seen in extreme discharges, rather than mid-segment discharges. Like BiasRR, BiasFMM reacts on changes of the long-term water balance. The BiasFMM is actually calculated for median discharges in the observed and simulated discharge values (probability 0.5). According to the results presented in Figure 6, BiasFMM is equal to 4.16% under the RCP2.6 scenario and 18.73% under the RCP8.5 scenario, that shows the median value has not changed significantly in the future. Moreover, the difference between BiasFMM values under these two scenarios is 14.56%, which is indicative of the range of difference between the discharges under these two scenarios. The Diffmaxpeak bias is actually calculated for the maximum observed and simulated discharge values. According to the results presented in Figure 6, Diffmaxpeak bias is equal to 47.08% under the RCP2.6 scenario and 144.81% under the RCP8.5 scenario. Since there is significant difference between the discharge values under these two scenarios (97.73%) it can be concluded that consideration of a maximum discharge instead of high-flow discharges is not a very good solution and researchers had better use BiasFHV in this case because it examines only one maximum value over a 30-year period. Nevertheless, this finding still confirms the rise in maximum discharges under the RCP8.5 scenario.

Each signature provides information about the intrinsic properties of the basin such as redistribution of soil moisture and long-term behavior of base flow. These indices, which are actually derived from FDCs, serve as a fingerprint revealing differences between the hydrological behaviors of the basin. Overall, these results show that average runoff will increase slightly in the future, which is greater for the RCP2.6 scenario. Why are some signature indices higher in RCP8.5? The answer to this question clarifies a more accurate understanding of future changes in the basin. The reason why the BiasRR has increased under the RCP8.5 scenario is because of the maximum discharges, which is due to this coefficient being affected by the mean flow. Increasing high flows are clearly shown in the FHV and Diffmaxpeak signatures. The reason why the annual average increases under the RCP2.6 scenario for FLV index can be explained as follows: first, the amount of low flows in the RCP2.6 scenario has increased; and, second, the amount of increasing temperature is less than the RCP8.5 in the future. Furthermore, the negative BiasFMS (probabilities between 20 and 70%) is the dominant behavior in the basin. These results including negative and positive values indicate the lack of uniform distribution of precipitation in the basin.

CONCLUSION

Development of industrial activities which is followed by overlooking of environmental issues has made the climate change effects more obvious than ever before and that is why this phenomenon is recognized as a global concern. Variations in temperature and precipitation patterns can significantly affect the quantity and quality of water resources, especially in arid and semi-arid regions. Therefore, study of basins' characteristics and the hydrological behavior of runoff is of vital importance. Taking this into account, it

can be argued that hydrological signatures that serve as a good instrument for describing the behavior of basins can be used as a perfect option for investigating the hydrological response of basins. Therefore, CanESM2 model and SDSM downscaling tools were used under the RCP2.6 and RCP8.5 scenarios to study the effect of climate change on temperature and precipitation parameters of Azarshahr Chay basin in 2030–2059. In the next step, the SWAT model was used to simulate surface runoff. Six signature indices (RR, FHV, FLV, FMS, FMM, and Diffmaxpeak) were used to investigate the hydrological behavior of the basin and reveal future hydrological changes arising from climate change.

The climate simulation results were indicative of optimal performance of the SDSM model in downscaling the large-scale data. Moreover, the calibration and validation results in the SWAT model (0.54 and 0.64 for the NSE) showed acceptable performance of the model. The average annual discharge for the future periods increased by 3.2 under the RCP2.6 scenario and by 2.1 under RCP8.5, but this rise was found to be less significant than annual discharge under the RCP8.5 scenario. However, signature bias studies revealed more interesting results that can provide further insight into the behavior of basins. The BiasRR which represents of overall runoff, was 9.265% and 34.95% higher under the RCP2.6 and RCP8.5 scenarios, respectively. The BiasFHV reached 31.18% and 94.55% under the RCP2.6 and RCP8.5 scenarios, respectively, and since this signature is provided for high flows, it can be argued that the number of high flows is higher under the pessimistic scenario (RCP8.5). This finding indicates that consideration of pessimistic conditions can lead to severe hydrological responses and extreme events such as floods in this signature. In other words, the average annual flow rate increases in comparison with the base period (the RCP8.5 scenario is +2.1% which is less than the RCP2.6 (+3.2%)). However, the average annual flow rate is lower in RCP8.5, the examination of the FHV index (percent bias in FDC high-segment volume) increases to a higher percentage in RCP8.5 (94.55%) than the base period and RCP2.6 (31.18%). BiasFLV (low discharges) was found to be 120.61% under the RCP2.6 scenario and 62.88% under the RCP8.5 scenario. This means that the low-flow volume is higher under the optimistic scenario, so it can be concluded that under the RCP8.5 scenario, bias in high flows and low flows are more significant than that in the baseline period and optimistic scenario. This is indicative of an increase in extreme events such as flood and drought. Interestingly, despite a less significant rise in the average 30-year discharge under the RCP8.5 scenario (as compared to the RCP2.6 scenario) it is believed that rises in discharge and, consequently, in probability of flood were more significant under the RCP2.6 scenario. The signatures showed that the most significant bias, under the RCP8.5 scenario, can be seen between signatures associated with high flow (FHV) and low flow (FLV), which can account for rises in annual flow and its lower value compared to that in the optimistic scenario. Similarly, the rise in FMM and Diffmaxpeak signatures were more significant than that in the baseline period under the RCP8.5 scenario and decline in flow rate was observed only in the FMS signature.

The results showed that signatures are useful instruments that can be used to evaluate changes in the future hydrological response of basins or to compare the basins with each other. The results also suggested that average annual and monthly changes (temperature, precipitation, runoff) alone cannot provide us with an inclusive account of future changes. Therefore, indices can be used as valuable instruments to address high to low flow changes, flood and drought, as well as the hydrological behavior of basins. However, it should be noted that more studies are needed for better understanding of the response of the basin, such as investigating unusually wet or dry periods.

DATA AVAILABILITY STATEMENT

Data cannot be made publicly available; readers should contact the corresponding author for details.

REFERENCES

Abbaspour, K. C., Faramarzi, M., Ghasemi, S. S. & Yang, H. 2009 Assessing the impact of climate change on water resources in Iran. *Water Resources Research* **45** (10), W10434. doi.org/10.1029/2008WR007615.

Blöschl, G., Sivapalan, M., Savenije, H., Wagener, T. & Viglione, A. (Eds.) 2013 *Runoff Prediction in Ungauged Basins: Synthesis Across Processes, Places and Scales*. Cambridge University Press, New York, USA.

Casper, M. C., Grigoryan, G., Gronz, O., Gutjahr, O., Heinemann, G., Ley, R. & Rock, A. 2011 Analysis of projected hydrological behavior of catchments based on signature indices. *Hydrology & Earth System Sciences Discussions* **8** (2), 571–597. doi.org/10.5194/hess-16-409-2012.

Dibike, Y. B. & Coulibaly, P. 2005 Hydrologic impact of climate change in the Saguenay watershed: comparison of downscaling methods and hydrologic models. *Hydrology* **307** (1–4), 145–163. doi.org/10.1016/j.jhydrol.2004.10.012.

Goodarzi, M. R., Fatehifar, A. & Moradi, A. 2020 Predicting future flood frequency under climate change using Copula function. *Water and Environment Journal* **34** (S1), 710–727. doi.org/10.1111/wej.1257.

Gunkel, A., Shadeed, S., Hartmann, A., Wagener, T. & Lange, J. 2015 Model signatures and aridity indices enhance the accuracy of water balance estimations in a data-scarce Eastern Mediterranean catchment. *Journal of Hydrology: Regional Studies* **4**, 487–501. doi.org/10.1016/j.ejrh.2015.08.002.

Gupta, H. V., Wagener, T. & Liu, Y. 2008 Reconciling theory with observations: elements of a diagnostic approach to model evaluation. *Hydrological Processes* **22** (18), 3802–3813. doi.org/10.1002/hyp.6989.

Herbst, M., Casper, M. C., Grundmann, J. & Buchholz, O. 2009 Comparative analysis of model behavior for flood prediction purposes using Self-Organizing Maps. *Natural Hazards and Earth System Sciences* **9**, 373–392. doi.org/10.5194/nhess-9-373-2009.

Intergovernmental Panel on Climate Change (IPCC) 2014 Climate Change 2014: Synthesis Report, Contribution of Working Groups I, II and III to the Fifth Assessment Report of the Intergovernmental Panel on Climate Change (Core Writing Team, R. K. Pachauri & L. A. Meyer, eds.). IPCC, Geneva, Switzerland, 151 pp. https://epic.awi.de/id/eprint/37530/

Juston, J., Jansson, P.-E. & Gustafsson, D. 2014 Rating curve uncertainty and change detection in discharge time series: case study with 44-year historic data from the Nyangores River, Kenya. *Hydrological Processes* **28** (4), 2509–2523. doi.org/10.1002/hyp.9786.

Kauffeldt, A., Halldin, S., Rodhe, A., Xu, C. Y. & Westerberg, I. K. 2013 Disinformative data in large-scale hydrological modelling. *Hydrology and Earth System Sciences* **17** (7), 2845–2857. https://doi.org/10.5194/hess-17-2845-2013.

Khan, A. J. & Koch, M. 2018 Selecting and downscaling a set of climate models for projecting climatic change for impact assessment in the upper Indus basin (UIB). *Climate* **6** (4), 89. doi.org/10.3390/cli6040089.

McDonnell, J. J. & Woods, R. 2004 On the need for catchment classification. *Journal of Hydrology* **299** (1), 2–3. doi.org/10.1016/j.jhydrol.2004.09.003.

McMillan, H. 2020 A review of hydrologic signatures and their applications. *Wiley Interdisciplinary Reviews: Water* **8** (1), e1499. doi.org/10.1002/wat2.1499.

McMillan, H., Westerberg, I. & Branger, F. 2017 Five guidelines for selecting hydrological signatures. *Hydrological Processes* **31** (26), 4757–4761. doi.org/10.1002/hyp.11300.

Mendoza, P. A., Mizukami, N., Ikeda, K., Clark, M. P., Gutmann, E. D., Arnold, J. R., Brekke, L. D. & Rajagopalan, B. 2016 Effects of different regional climate model resolution and forcing scales on projected hydrologic changes. *Journal of Hydrology* **541**, 1003–1019. 10.1016/j.jhydrol.2016.08.010.

Pervez, M. S. & Henebry, G. M. 2014 Projections of the Ganges–Brahmaputra precipitation downscaled from GCM predictors. *Journal of Hydrology* **517**, 120–134. doi:10.1016/j.jhydrol.05.016.

Sawicz, K., Wagener, T., Sivapalan, M., Troch, P. A. & Carrillo, G. 2011 Catchment classification: empirical analysis of hydrologic similarity based on catchment function in the eastern USA. *Hydrology & Earth System Sciences Discussions* **8** (3), 4495–4534. doi:10.5194/hessd-8-4495-2011.

Schaefli, B., Harman, C. J., Sivapalan, M. & Schymanski, S. J. 2011 HESS opinions: hydrologic predictions in a changing environment: behavioral modeling. *Hydrology and Earth System Sciences* **15** (2), 635–646.

Smakhtin, V. U. 2001 Low-flow hydrology: a review. *Journal of Hydrology* **240** (3–4), 147–186. doi.org/10.1016/S0022-1694(00)00340-1.

Wagener, T., Sivapalan, M., Troch, P. & Woods, R. 2007 Catchment classification and hydrologic similarity. *Geography Compass* **1** (4), 901–931. doi.org/10.1111/j.1749-8198.2007.00039.x.

Westerberg, I. K. & McMillan, H. K. 2015 Uncertainty in hydrological signatures. *Hydrology and Earth System Sciences* **19** (9), 3951–3968. doi:10.5194/hess-19-3951-2015.

Westerberg, I. K., Wagener, T., Coxon, G., McMillan, H. K., Castellarin, A., Montanari, A. & Freer, J. 2016 Uncertainty in hydrological signatures for gauged and ungauged catchments. *Water Resources Research* **52** (3), 1847–1865. doi.org/10.1002/2015WR017635.

Wilby, R. L., Dawson, C. W. & Barrow, E. M. 2002 SDSM – a decision support tool for the assessment of regional climate change impacts. *Environmental Modelling & Software* **17** (2), 147–159. doi.org/10.1016/S1364-8152(01)00060-3.

Wilby, R. L., Whitehead, P. G., Wade, A. J., Butterfield, D., Davis, R. J. & Watts, G. 2006 Integrated modelling of climate change impacts on water resources and quality in a lowland catchment: River Kennet, UK. *Hydrology* **330** (1–2), 204–220. doi.org/10.1016/j.jhydrol.2006.04.033.

Yilmaz, K. K., Gupta, H. V. & Wagener, T. 2008 A process-based diagnostic approach to model evaluation: application to the NWS distributed hydrologic model. *Water Resources Research* **44** (9), W09417. doi.org/10.1029/2007WR006716.

Zhang, Y., You, Q., Chen, C. & Ge, J. 2016 Impacts of climate change on streamflows under RCP scenarios: a case study in Xin River Basin, China. *Atmospheric Research* **178**, 521–534. doi.org/10.1016/j.atmosres.2016.04.018.

First received 15 October 2020; accepted in revised form 27 March 2021. Available online 28 April 2021